Solution Structure of a DNA Duplex Containing a Nitroxide Spin-Labeled Platinum d(GpG) Intrastrand Cross-Link Refined with NMR-Derived Long-Range Electron−Proton Distance Restraints

Shari U. Dunham,[†] Stephen U. Dunham,[†] Christopher J. Turner,[‡] and Stephen J. Lippard*,[†]

Contribution from the Department of Chemistry and the Francis Bitter Magnet Laboratory, Massachusetts Institute of Technology, Cambridge, Massachusetts 02139

Received December 16, 1997

Abstract: Modification of an undecamer deoxyribonucleotide, d(CTCTCGGTCTC), with the paramagnetic cisplatin analogue *cis*-[Pt(NH_3)(4AT)ClI] afforded two orientational isomers of the platinated DNA containing a site-specific intrastrand d(GpG) cross-link. The DNA strand containing the 3′ orientational isomer was annealed to its complement, and the resulting duplex was investigated by NMR spectroscopy. The structure was determined from conventional NOE studies of the reduced, diamagnetic undecamer and 99 long-range (10−20 Å) electron−proton restraints from the paramagnetic duplex. The platinum-modified duplex is substantially bent toward the major groove. Refinements of the structure with either conventional interproton restraints or a combination of the electron−proton and interproton restraints afforded the same local but different global structures. Both refinements resulted in duplexes that deviated from canonical B-form DNA with widened minor grooves. Addition of the long-range electron−proton restraints allowed for refinement of a duplex structure in excellent agreement with the diamagnetic NMR data (R-factor = 6.08) but exhibiting different positioning of the duplex ends. In particular, the long-range distance restraints afforded a refined duplex with marked similarity (RMSD for all backbone atoms = 1.98 Å) to the tertiary structure of a cisplatin-modified dodecamer duplex solved by X-ray crystallography (*J. Am. Chem. Soc.* **1996**, *118*, 12309−21321). The described approach, combining long-range electron−proton and short-range interproton distance restraints in DNA structure refinement, has improved our understanding of the delocalized nature of platinum-induced distortions in duplex DNA and may facilitate high-resolution structural studies of other distorted oligonucleotide duplexes.

Introduction

The mechanism of action of the anticancer drug *cis*-diamminedichloroplatinum(II),[1] or cisplatin,[2] involves binding to and concomitant structural distortion of DNA.[3] Elucidating the link between DNA structure modification and platinum-based antitumor function is a focus of many studies. The bifunctional intrastrand d(GpG) and d(ApG) DNA adducts, where platinum coordinates to the N7 positions of adjacent purine bases, have been the most extensively investigated since they comprise up to 90% of the DNA adducts formed in vivo.[4,5] In the present work, we have exploited the far-reaching effects of a paramagnetic nitroxide spin-labeled analogue of cisplatin to determine long-range electron−proton distance restraints to augment the refinement of a high-resolution solution NMR structure of such a platinum-modified DNA duplex.

High-resolution structures of cisplatin-modified duplex DNA are available, but are limited in their ability to address solution tertiary structure. An X-ray crystal structure of a cisplatin-modified dodecamer duplex, solved to 2.6 Å resolution, revealed details of the platinum d(GpG) cross-link and a double helix with an unusual A−B junction.[6,7] Both end-to-end (B−B) and end-to-groove (A−A) packing interactions occur in the crystal, accounting for the heterogeneity of the duplex.[7] In solution, where such crystal packing effects cannot occur, the same platinated DNA is significantly bent and distorted from the B-form DNA, although with predominantly B-type sugar puckers and intrastrand phosphate−phosphate distances.[8] The solution structure of a metastable cisplatin-modified octamer duplex has also been reported.[9] Both of these NMR-derived structures were refined with the benefit only of short-range NOE restraints. They accurately address local geometry but may not adequately characterize more global features such as the details of DNA duplex bending or unwinding.

[†] Department of Chemistry.

[‡] Francis Bitter Magnet Laboratory.

(1) Rosenberg, B.; VanCamp, L.; Trosko, J. E.; Mansour, V. H. *Nature* **1969**, *222*, 385.

(2) Abbreviations: cisplatin, *cis*-diamminedichloroplatinum(II); TEMPO, 2,2,6,6-tetramethylpiperidinyloxy; 4AT, 4-aminoTEMPO; TEMPOL, 4-hydroxyl-2,2,6,6-tetramethylpiperidinyloxy; DMF, *N*′,*N*′-dimethylformamide; NOE, nuclear Overhauser effect; NOESY, nuclear Overhauser effect spectroscopy; COSY, correlation spectroscopy; d_4-TSP, sodium 3-trimethylsilylpropionate-2,2,3,3-d_4; $CyNH_2$, cyclohexylamine; rMD, restrained molecular dynamics.

(3) Pil, P. M.; Lippard, S. J. In *Encyclopedia of Cancer*; Bertino, J. R., Ed.; Academic Press: San Diego, CA, 1997; Vol. 1, pp 392−410.

(4) Eastman, A. *Pharmacol. Ther.* **1987**, *34*, 155−166.

(5) Fichtinger-Schepman, A. M. J.; van der Veer, J. L.; den Hartog, J. H. J.; Lohman, P. H. M.; Reedijk, J. *Biochemistry* **1985**, *24*, 707−713.

(6) Takahara, P. M.; Rosenzweig, A. C.; Frederick, C. A.; Lippard, S. J. *Nature* **1995**, *377*, 649−652.

(7) Takahara, P. M.; Frederick, C. A.; Lippard, S. J. *J. Am. Chem. Soc.* **1996**, *118*, 12309−12321; **1997**, *119*, 14795.

(8) Gelasco, A. K.; Lippard, S. J. *Biochemistry* In press.

(9) Yang, D.; van Boom, S. S. G. E.; Reedijk, J.; van Boom, J. H.; Wang, A. H.-J. *Biochemistry* **1995**, *34*, 12912−12920.

S0002-7863(97)04259-5 CCC: $15.00
Published on Web 05/22/1998

NMR spectroscopy is the method of choice for investigating the structure and dynamics of biological macromolecules in solution. The NMR observables, including coupling constants, chemical shifts, residual dipolar splittings, and nuclear Overhauser effects (NOEs), are related to molecular structure. Although chemical shift[10] and residual dipolar splitting[11] of a magnetic nucleus can be quantitated, their ability to define the structure of a DNA duplex is limited,[10] and their inclusion in the iterative refinement of such structures is not yet routine.[12] Coupling constants afford torsion angles within DNA, but their quantitation and interpretation can be difficult.[13,14]

The most valuable NMR restraints for refining DNA structures are derived from the nuclear Overhauser effect. An NOE is the result of a dipolar interaction between two magnetic nuclei and exhibits an inverse sixth-root dependence on internuclear distance when cross-relaxation is negligible. The magnitude of the proton magnetic moment limits the interproton NOEs to distances of ≤ 5 Å. In globular macromolecules such as proteins, interproton distances of this magnitude occur within residues, between sequential adjacent residues, and, most important for characterizing tertiary structure, between nonsequential but proximal residues. NMR-derived restraints for extended polypeptides and, in particular, for duplex oligonucleotides are highly localized and suffer from the lack of tertiary structure to provide NOE restraints between nonnearest neighbor residues. Consequently, NMR structures of duplex oligonucleotides are underdetermined, making characterization of the overall shape or bend of the duplex a significant challenge.[15−17]

In the present investigation, we have addressed this problem by introducing a paramagnetic moiety into a site-specifically platinated DNA duplex. The platinum compound employed, *cis*-[Pt(NH_3)(4AT)ClI],[18] contains an unpaired electron localized on the organic nitroxide moiety of a 4AT (4-aminoTEMPO) ligand. This platinum compound is a structural analogue of *cis*-[Pt(NH_3)($CyNH_2$)Cl_2], the active metabolite of oral platinum(IV) antitumor agents.[19−21] The unpaired electron of the nitroxide spin label has a magnetic moment that is greater than 500 times that of a proton, allowing for effective electron−proton dipolar coupling over distances much greater than the 5 Å limit of NOEs. This technique of incorporating a site-specific, covalently attached nitroxide spin label to a biological macromolecule has previously been used to determine long-range (10−30 Å) distances in proteins.[22−25] The DNA system used in the present study, however, has several advantages as compared to these earlier protein studies, including the ease of incorporation of the spin label, the ability to purify the resulting products, and the conformational rigidity of the label when nestled in the major groove of the duplex. Previously, we used the paramagnetic properties of 4AT to provide structural information about *cis*-[Pt(NH_3)(4AT){d(GpG)}]$^+$.[18] Here we take advantage of the long-range electron−proton distance restraints to refine the related platinum-modified DNA undecamer duplex depicted in Figure 1.

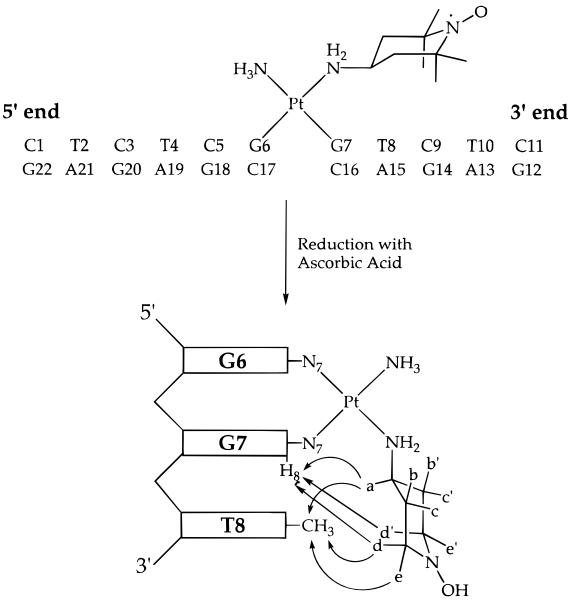

Figure 1. Schematic representation of the 3′ orientational isomer of ts11 modified with **1**. The oxidized and reduced forms of the 4-aminoTEMPO ligand are drawn, and observed TEMPO to DNA interproton NOEs are indicated by arrows.

Experimental Section

Synthesis, Platination, and Purification of Deoxyoligonucleotides. The deoxyribonucleotides d(CTCTCGGTCTC), ts11, and d(GAGACCGAGAG), bs11, were prepared in micromole quantities on a Cruachem PS250 DNA synthesizer by using phosphoramidite chemistry on a solid support. Deprotected oligonucleotides were initially purified by size exclusion chromatography (G25 Sephadex, Pharmacia). The unmodified oligonucleotide bs11 was purified either by preparative ion exchange HPLC (DIONEX, NucleoPac PA-100 9 × 250 mm column with a linear NaCl gradient in 0.025 M NH_4OAc, pH 6.0, 10% acetonitrile) or C_4 reversed phase HPLC (VYDAC, 22 × 250 mm column, with a nonlinear acetonitrile gradient in 0.1 M NH_4OAc, pH 6.0). Following reversed phase HPLC purification and prior to platinum modification, oligonucleotides were converted to their sodium forms by using cation exchange chromatography (DOWEX, Aldrich).

The compound *cis*-[Pt(NH_3)(4AT)ClI] was synthesized from the potassium or tetraphenylphosphonium salt of [Pt(NH_3)Cl_3]$^-$ [26] and 4-aminoTEMPO (4AT) (Aldrich) as previously described.[18] Oligonucleotides containing a single d(GpG) site for platinum modification were allowed to react with 1.0 to 1.5 equiv of the paramagnetic, doubly activated platinum species, *cis*-[Pt(NH_3)(4AT)X_2]$^{n+}$ (**1**), where X is DMF and/or NO_3^- and $0 \leq n \leq 2$.[18] Reactions were carried out in 10 mM sodium phosphate buffer, pH 6.0, at DNA strand concentrations of ≥ 10 μM for 2−20 h at 22 °C. Platination of ts11 was monitored by reversed phase HPLC (C_4, VYDAC, 4.6 × 250 mm column with linear gradients of acetonitrile in 0.1 M NH_4OAc, pH 6.0). Two major

(10) Wijmenga, S. S.; Mooren, M. M. W.; Hilbers, C. W. In, *NMR of Macromolecules*: *A Practical Approach*; Roberts, G. C. K., Ed.; Oxford University Press Inc.: New York, 1993.
(11) Bax, A.; Tjandra, N. *Nature Struct. Biol.* **1997**, *4*, 254.
(12) Kung, H. C.; Wang, K. Y.; Goljer, I.; Bolton, P. H. *J. Magn. Reson. B* **1995**, *109*, 323−325.
(13) Zhu, L.; Reid, B. R.; Kennedy, M.; Drobny, G. P. *J. Magn. Reson. A* **1994**, *111*, 195−202.
(14) Zhu, L.; Reid, B. R.; Drobny, G. P. *J. Magn. Reson. A* **1995**, *115*, 206−212.
(15) Brünger, A. T *X-PLOR, Version 3.1*: *A System for X-ray Crystallography and NMR*; Yale University Press: New Haven, CT, 1992.
(16) Goljer, I.; Bolton, P. H. In *Two-Dimensional NMR Spectroscopy*: *Applications for Chemists and Biochemists*; Croasmun, W. R., Carlson, R. M. K., Eds.; VCH Publishers: New York, 1994; pp 699−740.
(17) Wüthrich, K. *Acta Crystallogr.* **1995**, *D51*, 249−270.
(18) Dunham, S. U.; Lippard, S. J. *J. Am. Chem. Soc.* **1995**, *117*, 10702−10712.
(19) Hartwig, J. F.; Lippard, S. J. *J. Am. Chem. Soc.* **1992**, *114*, 5646−5654.
(20) Barnard, C. F. J.; Vollano, J. F.; Chaloner, P. A.; Dewa, S. Z. *Inorg. Chem.* **1996**, *35*, 3280−3284.
(21) Kelland, L. R.; Murrer, B. A.; Abel, G.; Giandomenico, C. M.; Mistry, P.; Harrap, K. R. *Cancer Res.* **1992**, *52*, 822−828.
(22) Kuntz, I. D.; Schmidt, P. G. *Biochemistry* **1984**, *23*, 4261−4266.
(23) Kosen, P. A. *Methods Enzymol.* **1989**, *177*, 86−121.
(24) Girvin, M. E.; Fillingame, R. H. *Biochemistry* **1994**, *33*, 665−674.
(25) Yu, L.; Meadows, R. P.; Wagner, R.; Fesik, S. W. *J. Magn. Reson. B* **1994**, *104*, 77−80.
(26) Giandomenico, C. M.; Abrams, M. J.; Murrer, B. A.; Vollano, J. F.; Rheinheimer, M. I.; Wyer, S. B.; Bossard, G. E.; Higgins III, J. D. *Inorg. Chem.* **1995**, *34*, 1015−1021.

products eluted sequentially from the column (ts11A and ts11B, respectively) and were separated and isolated by preparative HPLC (C_4, VYDAC, 22 × 250 mm column) with optimized gradient conditions.

Concentrations of ts11 and bs11 were determined from optical absorbance readings at 260 nm using estimated extinction coefficients of 90 000 M^{-1} cm^{-1} and 118 700 M^{-1} cm^{-1}, respectively.[27] The ratio of bound platinum per oligonucleotide was determined by optical spectroscopy and atomic absorption spectroscopy, the latter on a Varian 1475 atomic absorption spectrometer equipped with a graphite furnace and operating in peak height mode at 265.9 nm.

Annealed oligonucleotide duplexes were prepared by titrating bs11 into a buffered (100 mM NaCl, 10 mM sodium phosphate, pH 6.8) aqueous solution of ts11, ts11A or ts11B followed by moderate heating (37−45 °C for 5−15 min) and cooling over 5−10 h to room temperature or 4 °C. Duplex formation was monitored by ion exchange HPLC (DIONEX NucleoPac PA-100 4 × 250 mm column, with a linear NaCl gradient in 0.025 M NH_4OAc, pH 6.0, 10% acetonitrile). Paramagnetic duplexes ($ds11A_{para}$ and $ds11B_{para}$) were formed by annealing the isolated paramagnetic strands ($ts11A_{para}$ or $ts11B_{para}$) with 1.0 equiv of bs11. Diamagnetic oligonucleotides ($ts11A_{dia}$, $ts11B_{dia}$, $ds11A_{dia}$, and $ds11B_{dia}$) were prepared by ascorbic acid reduction (Figure 1), which converts the 4AT ligand from its paramagnetic nitroxide to the diamagnetic hydroxylamine form (4ATH).[18,23] Following reduction, ascorbic acid was removed either by size exclusion or reversed phase HPLC. Anaerobic conditions were required to maintain the modified DNAs in their reduced forms in buffered aqueous solution at room temperature.

Enzymatic Digestions. *NOTE*: *Extreme caution should be used when working with cyanide ion, which is a particularly hazardous substance*. Aliquots (1−5 nmol) of platinated single-stranded oligonucleotides were allowed to react with 25 units of P1 nuclease (GIBCO BRL) for 30 h at 37 °C in 100 mM NaOAc, pH 5.3. One-fourth of this solution (30 μL) was diluted 10-fold in 100 μM EDTA and 50 mM Tris-HCl, pH 8.5, and digested further with 4 units of alkaline phosphatase (Boehringer Mannheim) for 24 h at 37 °C. After enzymatic digestion, 1000−2000 equiv of sodium cyanide was allowed to react with an aliquot of the digested DNA solutions at 37 °C for several hours. All digested, cyanide reversed, and standard samples were analyzed by reversed phase HPLC under identical conditions (C_{18} 4.6 × 250 mm column, VYDAC, with a linear acetonitrile gradient in 0.1 M NH_4OAc, pH 6.0).

EPR and UV−Vis Spectroscopy. EPR spectra were recorded at 25 °C on an X-band Bruker ESP-300 spectrometer with the following parameters: 64−256 scans, 100 G sweep width centered at 3472 G, 1.0 G modulation amplitude, 100 kHz modulation frequency, 1.28 ms time constant, and 2 mW microwave power. Samples were dissolved in 80 μL of water, transferred to a 100 μL glass capillary in a 5 mm quartz tube for measurements, and externally referenced to a 1 mM aqueous sample of TEMPOL (Aldrich), $g = 2.006$.

Melting and cooling curves for the DNA duplexes (0.1−1.0 OD of DNA in 100 mM NaCl and 10 mM sodium phosphate buffer, pH 6.8) were obtained by optical absorption spectroscopy at 260 nm on an AVIV Model 14DS UV−vis spectrophotometer. Data were collected in 1 or 2° intervals between 5.5 and 55.5 °C with 2 min equilibration times and 1 s averaging at each step.

NMR Spectroscopy. Duplex oligonucleotides (0.5−3.0 μmol) were dissolved in 600 μL of 100 mM NaCl and 10 mM sodium phosphate, pH 6.8, with 0.1 mM d_4-TSP (Aldrich) as an internal chemical shift standard. After repeated lyophilization from 99.996% D_2O (Cambridge Isotopes Laboratories), samples were reconstituted in a 600 μL volume. For experiments involving exchangeable protons, samples were lyophilized and redissolved in 90% H_2O/10% D_2O.

1D proton NMR spectra of duplexes in D_2O buffer were acquired at 500 MHz on a Varian VXR spectrometer. Paramagnetic samples were studied at duplex concentrations below 1 mM in order to minimize intermolecular relaxation effects.[18] Longitudinal (T_1) and transverse (T_2) relaxation times were measured at 23 °C with the inversion recovery[28] and CPMG[29] pulse sequences, respectively. The intensity for each resolved proton signal as a function of delay time was fit to an exponential expression (VNMR version 5.1) to determine relaxation time values.

2D magnitude COSY spectra were also acquired at 500 MHz with 1024 complex points in t_2, 256 points in t_1, and presaturation of the residual water signal. All NOESY data were acquired on a 591 MHz home-built NMR spectrometer (Francis Bitter Magnet Laboratory). A series of phase sensitive NOESY spectra in D_2O buffer were acquired at 23 °C with 4096 complex points in t_2, 512 points in t_1, and 6000 Hz sweep width in each dimension. Data were collected with five mixing times (80, 100, 150, 200, and 400 ms) for a 3−4 mM sample of $ds11B_{dia}$ and with two mixing times (200 and 400 ms) for a ≤1 mM sample of $ds11B_{para}$. NOESY spectra in H_2O buffer were recorded at 10 °C on a 591 MHz spectrometer with 50, 100, and 300 ms mixing times, WATERGATE[30] minimization of the water signal, 4096 complex points in t_2, 512 points in t_1, and 12 000 Hz sweep width in each dimension. Data were transferred to a Silicon Graphics workstation and processed in Felix (version 95.0, Biosym Technologies). NOESY data were processed with 5 Hz exponential line broadening in both dimensions, and data in the t_1 domain were zero-filled to 4096 points. For all spectra, the first data point was divided by 2 so as to reduce t_1 noise, and a polynomial baseline correction was applied in the t_2 domain.

Diamagnetic Restraints. For initial structure refinements, the deoxyribose sugars in two residues with strong cross-peak intensities in the H8/H6 to H3′ region of the 80 ms D_2O NOESY spectrum were restrained with standard $C_{3'}$-endo dihedral angles. Seventeen residues with very little intensity in this region were restrained with standard $C_{2'}$-endo dihedral angles, and no dihedral angle restraints were applied to three residues with moderate intensity in this region.

NOESY cross-peak volumes were quantitated in Felix (version 95.0, Biosym Technologies). For each isolated and assigned cross-peak, the volume in a standard area was determined. For initial interproton distance restraints, the cross-peak volume in the 200 ms NOESY spectrum of $ds11B_{red}$ was converted to a proton−proton distance by using the isolated spin pair approximation.[31] In this approximation, the thymidine methyl-to-H6 interaction (2.88 Å), the TEMPO geminal methyl-to-methyl interaction (3.05 Å), and the cytidine H5-to-H6 interaction (2.49 Å) were used to calibrate the methyl-to-proton, methyl-to-methyl, and all other interproton volumes, respectively.

Restraints corresponding to standard hydrogen-bonding distances[16] were applied to those base pairs for which an imino proton was observable, assignable, and exhibited NOE interactions with either the H2 of adenine or the amino protons of cytidine. In those base pairs for which the imino proton was not assignable owing to lack of NOESY cross-peaks (C1-G22, G6-C17, and C11-G12, Figure 1), hydrogen bonding was more loosely restrained (1.8−2.4 Å). NOESY cross-peaks between an exchangeable proton in one base and a proton in another base pair, when observed, were converted to distance restraints with a 3.0−5.0 Å range. Weak cross-peaks between aromatic protons in consecutive bases in a strand, *n*H8/H6 to (*n*+1)H8/H6, excluding the very strong G6 H8 to G7 H8 interaction, if observable in the 300 ms NOESY spectrum in H_2O buffer, were also given 3.0−5.0 Å distance bounds.

Paramagnetic Distance Restraints. In this system, an unpaired electron is localized on the nitrogen atom of the nitroxide moiety. The distance from the unpaired electron to a specific proton nucleus can be determined from the paramagnetic contribution to the proton nuclear relaxation rate. The paramagnetic contribution (T_p^{-1}) to either the longitudinal (T_1^{-1}) or transverse (T_2^{-1}) relaxation rate of a magnetic nucleus is proportional to $1/r$,[6] where r is the electron−proton distance.

The relaxation rate for a proton in $ds11B_{para}$ (T_{obs}^{-1}) is the sum of both diamagnetic (T_{dia}^{-1}) and paramagnetic (T_{para}^{-1}) contributions (eq 1). Since T_{dia}^{-1} can be directly determined as the relaxation rate of the proton in $ds11B_{dia}$, T_{para}^{-1} can be calculated as the change in

(27) Borer, P. N. In *Handbook of Biochemistry and Molecular Biology*; Fasman, G. D., Ed.; CRC Press: Cleveland, OH, 1975; Vol. 1, pp 589−589.

(28) Vold, R. L.; Waugh, J. S.; Klein, M. P.; Phelps, D. E. *J. Chem. Phys.* **1968**, *48*, 3831−3832.

(29) Meiboom, S.; Gill, D. *Rev. Sci. Instrum.* **1958**, *29*, 688.

(30) Sklenar, V.; Piotto, M.; Leppik, R.; Saudek, V. *J. Magn. Reson. A* **1993**, *102*, 241−245.

(31) Clore, G. M.; Gronenborn, A. M. *FEBS Lett.* **1985**, *179*, 187−198.

$$\frac{1}{T_{obs}} = \frac{1}{T_{dia}} + \frac{1}{T_{para}} \quad (1)$$

relaxation rate in the absence of intermolecular relaxation by using eq 1. For proton nuclei at high magnetic field strengths, where the Larmour frequency of the electron, ω_S, is much larger than the Larmour frequency of the nucleus, ω_I, the Solomon−Bloembergen[32] equations, which relate the paramagnetic contribution of nuclear relaxation rate to electron−proton distance, can be simplified as indicated in eqs 2 and 3.[23] A correlation time of each electron−proton vector, τ_{c1}, is

$$\frac{1}{T_{1para}} = \frac{2.46 \times 10^{-32}\ \mathrm{cm^6\ s^{-2}}}{r^6}\left(\frac{3\tau_{c1}}{1+\omega_I^2\tau_{c1}^2}\right) \quad (2)$$

$$\frac{1}{T_{2para}} = \frac{1.23 \times 10^{-32}\ \mathrm{cm^6\ s^{-2}}}{r^6}\left(4\tau_c + \frac{3\tau_{c1}}{1+\omega_I^2\tau_{c1}^2}\right) \quad (3)$$

determined from the ratio ($T_{1para}^{-1}/T_{2para}^{-1}$) for each resolved proton in a 1D spectrum (eq 4). Correlation times (τ_{c1}) and paramagnetic

$$\frac{T_{1para}^{-1}}{T_{2para}^{-1}} = 2\left(\frac{3\tau_{c1}}{1+\omega_I^2\tau_{c1}^2}\right)\Big/\left(4t_{c1} + \frac{3\tau_{c1}}{1+\omega_I^2\tau_{c1}^2}\right) \quad (4)$$

relaxation rates (T_{1para}^{-1} and T_{2para}^{-1}) were then used in eqs 2 and 3 to determine electron−proton distances for protons resolved in the 1D ^{1}H NMR spectrum. These distances were employed in the scaling of the paramagnetic distances determined from 2D spectra, as described in the next section.

Additional long-range electron−proton distance restraints were estimated from the paramagnetic effect on NOESY cross-peak intensities. Each cross-peak in a NOESY spectrum, which results from the dipolar transfer of magnetization between two magnetically inequivalent nuclei (i and j) is affected by the relaxation rates (T_i^{-1} and T_j^{-1}) of both nuclei. Although the longitudinal (T_1) relaxation times of both i and j are active in the buildup and decay of a NOESY cross-peak,[33,34] the paramagnetic contribution to longitudinal relaxation rate (T_{1para}^{-1}), particularly for moderate to long electron−proton distances (>10 Å), approaches zero at high field strengths (eq 2). The paramagnetic contribution to T_{2para}^{-1}, however, approaches a constant value governed by $4\tau_c$ under these conditions (eq 3). Therefore, for electron−proton distances ≥10 Å at 600 MHz, the paramagnetic contribution to transverse relaxation rate (T_{2para}^{-1}), operative during the frequency selection and acquisition time domains, will dominate proton relaxation in the NOESY spectrum (Figure S1, Supporting Information).

As previously described,[23] the fractional change in intensity of an NMR signal, assuming T_2 relaxation is dominant, also represents the fractional change in T_2 (eq 5). Therefore, for a known T_{2dia} and a given

$$\frac{I_{dia} - I_{obs}}{I_{dia}} = \frac{T_{2dia} - T_{2obs}}{T_{2dia}} \quad (5)$$

τ_{c1} value, the change in NOESY cross-peak intensity can be used in eqs 1, 3, and 5 to determine the electron−proton distance. The resulting relationship between change in NOESY cross-peak intensity and electron−proton distance is plotted in Figure 2 for a proton with a T_{2dia} of 0.15 s and τ_c of 4.5 ns. In the present study, volumes in a standard sized area (2 Hz × 2 Hz) were quantitated for all resolved cross-peaks in selected regions of the 200 ms NOESY spectra of ds11B$_{dia}$ and ds11B$_{para}$. The paramagnetic cross-peak intensity was scaled until the fractional change in intensity (eq 5) for cross-peaks containing reference protons (A19 H8, A21 H8, G22 H8, T2 CH_3, and C16 H6) agreed with the electron−proton distances as determined from 1D experiments. Cross-peaks arising from interactions with A21 H2

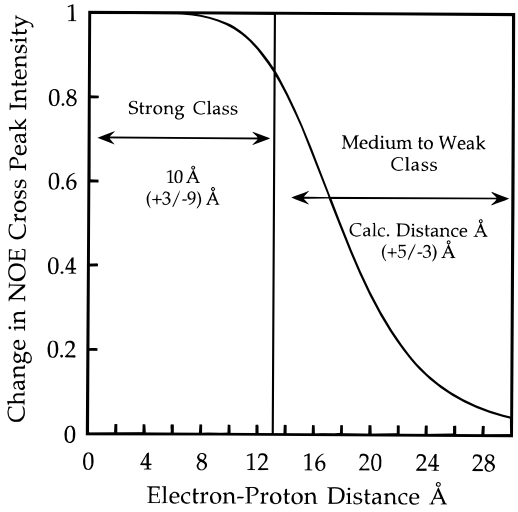

Figure 2. Change in NOESY cross-peak intensity plotted versus the electron−proton distance for a proton with a 0.15 s T_{2dia} and a 4.5 ns correlation time.

were not used in this scaling owing to the weakness of their intensities in the NOESY spectra of ds11B$_{dia}$.

For structure refinements, the resulting electron−proton distance restraints were applied between a given proton and the nitroxide nitrogen atom of the 4AT ligand. Typically, 3−5 NOESY volumes were averaged for each assigned proton. Protons having cross-peaks exhibiting >95% loss in volume (strong class in Figure 2, 40 restraints) were assigned an electron−proton distance of ≤13 Å. All distances in the medium to weak class (Figure 2, 59 restraints) were assigned conservative bounds of +5 and −3 Å from the calculated distance. The asymmetry of these bounds accounts for the potential underestimation of electron−proton distances due to the interproton distances that give rise to each NOESY cross-peak.[23] The magnitudes of these conservative ranges were tested in refinements with more restrictive bounds (+3Å, −1Å), resulting in little change in the final structures but a moderate (∼10%) increase in energy associated with the violation of interproton distance restraints.

Structure Refinement. Restrained molecular dynamics (rMD) simulations were performed in XPLOR[15] with the parallhdg.dna force field modified with parameters for the {Pt(NH$_3$)(4AT)}$^{2+}$ moiety and the coordinated guanosine residues as previously described.[18] The scaling of bonds, angles, dihedral angles, and improper angles in this force field was also applied to the added platinum parameters to reflect the requirements of structure refinement with interproton distance restraints.[15] Improper angles that maintain the coplanarity of the individual platinated guanine bases with the Pt−N7 bond were removed.[7] Simulations were carried out in a vacuum with a distance-dependent dielectric, reduced phosphate charge and an 11.5 Å cutoff for nonbonded interactions.

NMR-derived structure restraints were applied to ds11B in two starting structures, canonical A-form or B-form DNA. Starting structures were generated in QUANTA (version 4.1, Molecular Simulations Inc.), where the energy-minimized {*cis*-Pt(NH$_3$)(4AT)}$^{2+}$ moiety was docked at a position ∼2 Å from the N7 positions of G6 and G7. Conjugate gradient minimization (2000 cycles) was performed on each of these structures prior to 20 ps of restrained molecular dynamics (rMD) in 0.5 fs steps at 300 K. All distance restraints were applied with a square-well potential energy function. Coordinates of the final 2 ps of the dynamics trajectory were averaged, subjected to a maximum of 2000 cycles of conjugate gradient minimization, and submitted for another such rMD cycle. After 3−5 rMD cycles, structures resulting from A-form and B-form duplexes were converged (RMSD < 1.2 Å for all non-hydrogen atoms). Converged structures were then subjected to molecular dynamics restrained by the full relaxation matrix approach[35] from 400 to 100 K in 0.5 fs time steps

(32) Solomon, I. *Phys. Rev.* **1955**, *99*, 559−565.
(33) Bertini, I.; Luchinat, C. *Coord. Chem. Rev.* **1996**, *150*, 163−184.
(34) La Mar, G. N.; de Ropp, J. S. In *Biological Magnetic Resonance*: *NMR of Paramagnetic Molecules*; Berliner, L. J., Reuben, J., Eds.; Plenum Press: New York, 1993; Vol. 12.
(35) Nilges, M.; Habazettl, J.; Brünger, A. T.; Holak, T. A. *J. Mol. Biol.* **1991**, *219*, 499−510.

Table 1. Proton Chemical Shifts (ppm) and Assignments in 3′ds11$_{dia}$[a]

residue	H1′	H2′	H2″	H3′	H4′	H6/H8	H5/H2/CH$_3$	NH$_b$/NH$_{nb}$[b]	H1/H3
C1	5.90	2.26	2.61	4.70	4.14	7.91	5.98	7.90/7.30	
T2	6.20	2.36	2.63	4.95	4.31	7.68	1.70		14.02
C3	6.05	2.22	2.56	4.82	4.24	7.67	5.70	8.51/7.20	
T4	5.97	2.20	2.49	4.86	4.19	7.47	1.67		13.92
C5	5.92	1.60	2.45	4.76	4.09	7.47	5.68	8.84/7.32	
G6	6.07	2.46	2.71	5.13	4.23	8.73			*d*
G7	5.57	2.25	2.45	4.68	4.20	8.36			13.36
T8	6.22	2.32	2.60	4.93	4.28	7.50	1.37		13.63
C9	6.07	2.20	2.56	4.83	4.19	7.65	5.68	8.51/7.24	
T10	6.15	2.21	2.53	4.91	4.19	7.50	1.77		14.12
C11	6.31	2.31	2.31	4.61	4.06	7.69	5.87	8.37/7.60	
G12	5.56	2.46	2.66	4.83	3.66	7.86			*d*
A13	5.93	2.77	2.85	5.06	4.42	8.19	7.80		
G14	5.60	2.64	2.75	5.04	4.42	7.78			12.77
A15	6.31	2.69	2.95	5.05	4.49	8.16	7.97		
C16	5.87	2.00	2.35	*d*	4.12	7.36	5.50	8.37/7.11	
C17	5.58	1.95	2.26	4.83	4.07	7.45	5.47	8.06/6.86	
G18	5.54	2.70	2.81	5.00	4.30	7.88			12.60
A19	5.97	2.67	2.85	5.06	4.41	8.09	7.61		
G20	5.43	2.54	2.67	4.99	4.34	7.69			12.75
A21	6.12	2.61	2.89	5.02	4.44	8.04	7.83		
G22	6.01	2.39	2.27	4.63	4.18	7.63			*d*

TEMPO[c]	Ha	Hb	Hb′	Hc	Hc′	CH$_3$d	CH$_3$d′	CH$_{3e}$	CH$_3$e′
	2.93	2.35	2.38	1.62	1.65	1.16	1.13	1.25	1.28

[a] Chemical shifts were measured at 23 °C and internally referenced to d_4-TSP at 0.0 ppm. [b] The abbreviations NH$_b$ and NH$_{nb}$ refer to the hydrogen-bonded and non-hydrogen-bonded amino protons in cytosine. [c] Letter designations of protons as shown in Figure 1. [d] Not assigned.

and 10 K temperature steps over 5 ps with an optimal correlation time of 7 ns as determined from a grid search. The weight of the relaxation matrix and hydrogen-bonding restraints were held constant throughout the refinement.

Analysis of Refined Structures. All structures were viewed and compared in QUANTA (version 4.1, Molecular Simulations Inc.). Helical parameters of final structures were determined in CURVES, version 5.1.[36,37] Final duplex structures were used to back-calculate regions of the 200 ms D_2O NOESY spectrum in the NMR module of QUANTA with a 7 ns correlation time, a leakage rate of 0.9 s^{-1}, and a recycle delay of 3.5 s. Back-calculated spectra were then visualized and compared in NMRCOMPASS (version 2.5.1, Molecular Simulations Inc.).

Results

Synthesis, Separation, and Identification of Orientational Isomers. As described previously,[18,19] two orientational isomers result when a mixed amine platinum compound forms a bifunctional d(GpG) adduct on DNA. In the 5′ isomer, the substituted amine is proximal to the 5′ guanosine, whereas in the 3′ isomer (Figure 1), the substituted amine is proximal to the 3′ guanosine. Modification of d(CTCTCGGTCTC) with **1** yields two products, ts11A and ts11B, in a 1:2 ratio that can be separated by HPLC (Figure S2). Both of these products contain 1 equiv of platinum per DNA strand, as determined by atomic absorption spectroscopy, and exhibit three-line EPR signals ($g = 2.006$, $A = 17$ G, Figure S3) arising from the nitroxide spin label.[38]

To confirm the bifunctional nature of the platinum adducts[39,40] and to identify the orientational isomers,[19] both ts11A$_{dia}$ and ts11B$_{dia}$ were subjected to enzymatic digestion analysis according to a published protocol.[39] Digestion of both ts11A$_{dia}$ and ts11B$_{dia}$ resulted in dC and dT monomer components as well as a single peak eluting later with a different retention time depending on the starting oligonucleotide (Figure S4). Following cyanide reversal of these digested samples, co-injections with an authentic standard confirmed that the most slowly eluting peak in the HPLC trace corresponded to d(GGT). Identification of ts11A$_{dia}$ as the 5′ isomer and ts11B$_{dia}$ as the 3′ isomer was possible by comparison with the HPLC traces of authentic standards prepared from d(GGT) and **1**. These assignments were further supported by the observed NOESY connectivities between the 4ATH ligand and base residues 3′ to the lesion in ds11B$_{dia}$, shown schematically in Figure 1.

Thermal Stability of Modified Duplexes. Derivative plots of the melting and cooling curves for ts11B plus 1 equiv of bs11 revealed a T_m of ∼30 °C (Figure S5). The ∼29 °C T_m value of ts11A plus 1 equiv of bs11 was virtually identical. Corresponding studies with the unmodified duplex yielded a T_m ∼ 54 °C. These results indicate that, although the bifunctional platinum lesion destabilizes the DNA duplex as previously described,[41] the orientation of the 4AT ligand does not affect the overall duplex stability.

NMR Studies. (A) Nonexchangeable Protons. The nonexchangeable protons in ds11B$_{dia}$ were assigned from COSY and NOESY spectral data by following standard procedures.[10] Assignments are given in Table 1. Aromatic H8/H6 to sugar H1′ connectivities could be traced without interruption through the unmodified strand d(GAGACCGAGAG) (Figure S6A). The corresponding NOESY connectivity along the modified strand (Figure S6B) was more challenging, because of overlap in the aromatic proton region at T2/C3 and T4/C5 base steps and a very weak G6 H1′ to G7 H8 cross-peak. All aromatic-to-aromatic proton connectivities were of very weak intensity except for a strong NOESY cross-peak between the H8 protons of the adjacent platinum-modified guanosines.

The four adenosine H2 protons were readily identified by their long relaxation times in the 1D inversion recovery

(36) Lavery, R.; Sklénar, H. *J. Biomol. Struct. Dyn.* **1988**, *6*, 63−91.
(37) Lavery, R.; Sklénar, H. *J. Biomol. Struct. Dyn.* **1989**, *6*, 655−667.
(38) *Spin Labeling*: *Theory and Applications*; Berliner, L. J., Ed.; Academic Press: New York, 1976.
(39) Eastman, A. *Biochemistry* **1986**, *25*, 3912−3915.
(40) Bellon, S. F.; Lippard, S. J. *Biophys. Chem.* **1990**, *35*, 179−188.
(41) Poklar, N.; Pilch, D. S.; Lippard, S. J.; Redding, E. A.; Dunham, S. U.; Breslauer, K. J. *Proc. Nat. Acad. Sci. U.S.A.* **1996**, *93*, 7606−7611.

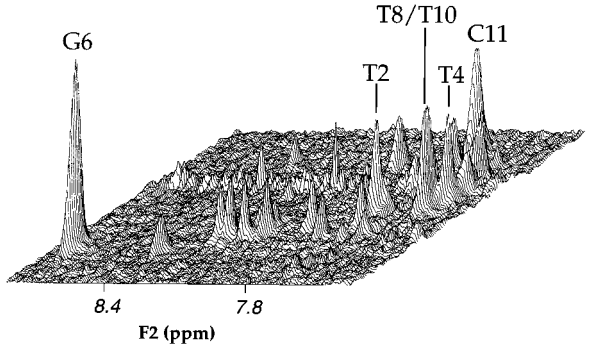

Figure 3. Stack plot of the *n*H8/H6 to *n*H3′ region of the 80 ms NOESY spectrum of 3′ds11$_{dia}$. Peaks with moderate to strong intensities are labeled.

experiment. Assignments for these resonances were possible from intraresidue H2 to H1′ connectivities observed in the 200 ms D_2O NOESY spectrum (Figure S6C). In addition, several other weak to moderate H2 cross-peaks were observed, including intrastrand *n*H2 to (*n*+1)H1′ cross-peaks and interstrand *n*H2 to (*m*+1)H1′ cross-peaks (Figure S6C).

Stereochemical assignments of the sugar H2′ and H2″ protons were determined from NOESY cross-peak intensity in the H1′ to H2′/H2″ region of the 80 ms D_2O NOESY spectrum. In this region, when mixing times are short and spin diffusion is not dominant, the H1′ cross-peak with H2″ is larger than that with H2′ for almost all pseudorotation angles of the deoxyribose ring.[10]

The *n*(H8/H6) to *n*(H3′) cross-peak intensity in the 80 ms NOESY spectrum was used as an indicator of deoxyribose sugar pucker.[10] When the deoxyribose ring adopts predominantly an N-type conformation, the H8/H6 to H3′ distance is ∼2.8−3.0 Å, whereas a longer distance (∼4−4.4 Å) results from an S-type sugar pucker. In ds11B$_{dia}$, the most intense cross-peaks in this aromatic to H3′ region are for residues G6 and C11 (Figure 3). Moderate intensities were observed for the T2, T4, and T10 residues, but little or no cross-peak intensity was observed in this region for the remaining residues of ds11B$_{dia}$.

All nonexchangeable protons of the reduced 4-aminoTEMPO ligand (4ATH) of ds11B$_{dia}$ could be assigned on the basis of both NOESY and COSY connectivities (Table 1, Figure S7). Stereospecific assignments were possible for all 4ATH protons in ds11B$_{dia}$ since each magnetically inequivalent proton nucleus has a unique chemical shift. This situation contrasts with that for 3′ or 5′ *cis*-[Pt(NH$_3$)(4ATH){d(GpG)}]$^+$, the dinucleotide model compounds, where chemical shifts for chemically equivalent but magnetically inequivalent nuclei were degenerate even at high fields.[18] Multiple intraligand connectivities were observed in the NOESY spectrum (Figure S7), including strong Ha-CH$_3$d′ and Ha-CH$_3$d cross-peaks as well as weak Ha-CH$_3$e and Ha-CH$_3$e′ cross-peaks, indicating a chair conformation of the six-membered TEMPO ring. In addition, strong 1D NOEs were observed between G7 H8 and the CH$_3$d and CH$_3$d′ of the 4AT ligand. These NOEs, in addition to other TEMPO-DNA connectivities (Figure 1), were also detected in the 2D NOESY experiment. The stereospecific chemical shifts of the 4ATH protons in ds11B$_{dia}$, combined with distinct intra- and interresidue NOESY connectivities for this ligand, allow one to fix the orientation of 4ATH with respect to the DNA duplex and reveal that the motion of this ligand is minimal on the NMR time scale. Analysis of the relative intensity of the EPR spectral components ($M = 0, \pm 1$) and the line width of the $M = 0$ component in the 25 °C spectrum of 3′ds11$_{para}$ (Figure S3) indicated the

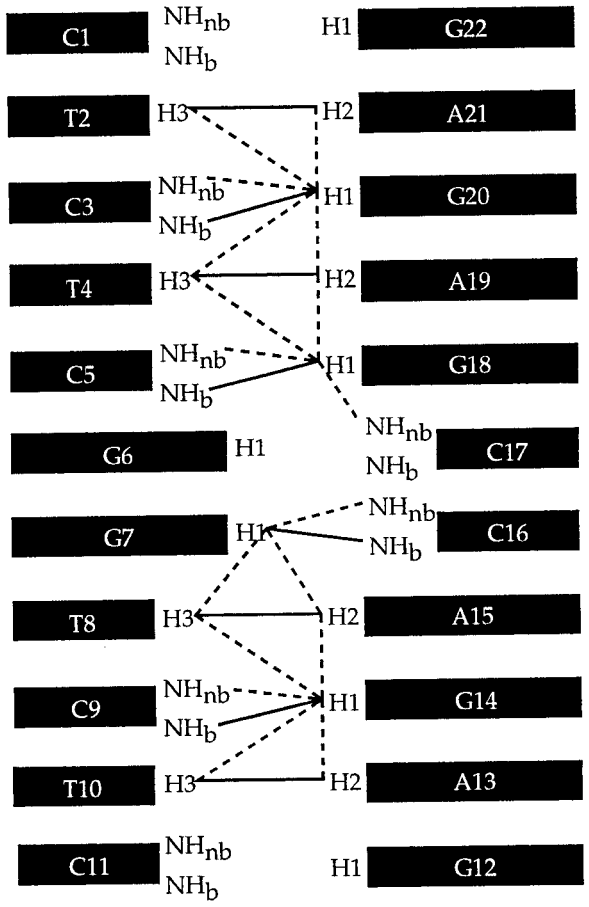

Figure 4. Schematic representation of interresidue connectivities observed for exchangeable protons in the 300 ms H_2O NOESY spectrum of 3′ds11$_{dia}$. Solid and dashed lines indicate strong and medium/weak intensities, respectively.

rotational correlation time of the spin label to be ∼4.4 ns, in the range (4.2−6.3 ns) expected for an 11 bp duplex.[38,42]

(B) Exchangeable Protons. Assignments of the imino (G H1 and T H3) and amino (C NH$_b$ and C NH$_{nb}$) protons in ds11B$_{dia}$ (Table 1) were based upon observed NOESY connectivities with previously assigned nonexchangeable protons (A H2 and C H5). Although 11 imino protons were recorded in the hydrogen-bonded region of the 1D ^{1}H NMR spectrum (Figure S8), only eight of these exchangeable protons exhibited cross-peaks in the H_2O NOESY spectra. The three imino protons for which cross-peaks could not be observed include those in the two terminal base pairs (G22 H1 and G12 H1) and an internal imino proton near the platinum coordination site (G6 H1). The hydrogen-bonded (NH$_b$) and nonbonded (NH$_{nb}$) amino protons of the cytosine residues involved in these base pairs (C1, C11, and C17) could be assigned however. In the 300 ms H_2O NOESY spectrum, imino-to-imino connectivities are obtained for base pairs T2-A21 to C5-G18 and again for G7-C16 to T10-A13 (Figure 4). Only the lack of the G6 imino resonance interrupts the connection between these two segments.

The strongest peaks in the imino-to-aromatic region of the 300 ms H_2O NOESY spectrum are thymidine H3 to adenine H2 and guanosine H1 to cytidine NH$_b$ cross-peaks (Figure S9). Several other moderate to weak cross-peaks are evident in this region at longer mixing times, the most interesting of which include a weak G18 H1 to C17 NH$_{nb}$ cross-peak and a cross-peak of moderate intensity between G7 H1 and an exchangeable

(42) Spaltenstein, A.; Robinson, B. H.; Hopkins, P. B. *J. Am. Chem. Soc*. **1989**, *111*, 2303.

Table 2. Paramagnetic ^{1}H Relaxation Times, Unique ^{1}H-^{1}H Correlation Times, and Electron−Proton Distances Determined for Six Resolved Protons in 3′ds11$_{dia}$[a]

proton	T_{1para} (s)	T_{2para} (s)	$10^9 \times \tau_{c1}$ (s)	1D electron−^{1}H distance (Å)	2D electron−^{1}H distance range (Å)
A19 H8	6.4 ± 2.4	0.085 ± 0.015	3.5	15.5 ± 1.7	13.5−21.5
A21 H8	7.0 ± 2.5	0.110 ± 0.032	3.1	16.0 ± 1.7	13.4−21.4
A21 H2	7.8 ± 1.8	0.102 ± 0.017	3.4	16.0 ± 1.1	10.7−18.7
G22 H8	8.0 ± 2.0	0.052 ± 0.006	4.9	15.2 ± 1.1	13.6−21.6
C16 H6	1.5 ± 0.3	0.018 ± 0.003	3.4	12.1 ± 0.7	9.5−17.5
T2 CH_3	11.9 ± 1.1	0.041 ± 0.008	6.6	15.4 ± 0.9	12.8−20.8

[a] Errors are reported as ± 2 standard deviations.

proton at 8.68 ppm (Figure S9). Since no other cross-peaks are observed to the resonance at 8.68 ppm, the proton assignment has not been determined. The unidentified resonance is most likely a hydrogen-bonded amino proton of a guanosine or adenosine residue, the orientation with reference to G7, and/or the water exchange rate, of which has drastically changed due to platinum-induced distortions of the duplex. Observed interproton connectivities involving exchangeable protons in ds11B$_{dia}$ are schematically depicted in Figure 4.

(C) Structural Implications of Diamagnetic NMR Data. Although the platinum-modified undecamer forms a stable duplex, the NMR data reveal distortions from canonical B-form DNA. The strong NOE between G6 H8 and G7 H8 is diagnostic of the destacking of the two purine bases due to platinum coordination at the N7 positions.[43] The sugars of two residues (G6 and C11) are predominantly in the N-type ($C_{3'}$-endo) conformation. This conformation, which predominates in A-form duplexes, is not uncommon at 3′ terminal residues and was one of the first characteristics to be identified for the 5′ purine nucleoside in bifunctional platinated 1,2-intrastrand cross-links.[43−45] Although all expected intra- and interresidue H6/H8 to H1′ cross-peaks were observed for ds11B$_{dia}$, some intensities were much weaker than would be expected for a canonical B-DNA duplex, for example, G6 H1′ to G7 H8.

The schematic in Figure 4 clearly illustrates the lack of exchangeable proton connectivities at the center of the platinum-modified duplex. The absence of cross-peaks to the imino proton of G6, even at 10 °C, indicates that the G6-C17 bp is very accessible to water. Although the G7-C16 and T8-A15 base pairs exhibit the expected intra- and interresidue exchangeable proton connectivities, many of these cross-peaks are relatively weak, suggesting only moderate stability. In addition, the medium intensities of the *n*A H2 to (*m*+1)H1′ interstrand cross-peaks suggest distortion of the DNA duplex. These cross-peaks have previously been identified as potential indicators of minor groove width deviations and base pair propeller twisting present in bent DNA structures.[16]

(D) Paramagnetic Effect on NMR Spectra of ds11B. Because there is minimal anisotropy in the electronic *g*-factor of the unpaired electron in the nitroxide spin label,[38] significant proton chemical shift changes between the diamagnetic and paramagnetic forms of ds11B do not occur. As a consequence, simply overlaying the assigned diamagnetic spectrum and the corresponding region of the paramagnetic spectrum allows for proton chemical shifts in ds11B$_{para}$ to be assigned. Because of the relatively slow relaxation of the nitroxide radical,[38,46] effective dipolar coupling with nuclear transitions occurs, resulting in a distance-dependent broadening of proton NMR signals. An example is shown in Figure 5 for the aromatic region of the 1D ^{1}H NMR spectra of ds11B$_{para}$ and ds11B$_{dia}$. In the paramagnetic duplex, signals from aromatic resonances close to the 4AT ligand cannot be detected, whereas signals from resonances farthest from the unpaired electron are still observable. Quantitation of this distance-dependent relaxation was carried out, and the resulting T_{1para} and T_{2para} relaxation times for those protons that are well resolved in the 1D spectrum of ds11B$_{dia}$ and still observed in ds11B$_{para}$ are reported in Table 2. Also given in this table are the τ_c values calculated from T_{1para} and T_{2para} by using eq 4 and electron−proton distances calculated according to eqs 2 and 3. Although the T_{1para} values for most of the protons in this table approach T_{1dia}, the calculated τ_c values are in agreement with the correlation times of both the nitroxide moiety and an 11 bp DNA duplex, as described above. In addition, errors in the electron−proton correlation times (±2 ns) are tolerable within the conservative bounds of the long-range electron−proton distances.

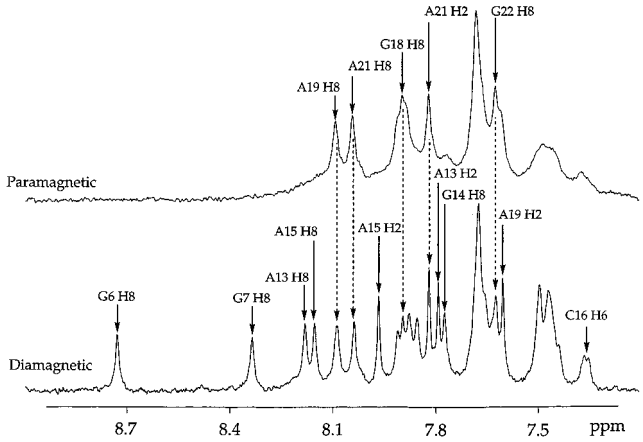

Figure 5. Overlay of the aromatic region of the 1D ^{1}H NMR spectra of 3′ds11$_{para}$ (top) and 3′ds11$_{dia}$ (bottom). Proton chemical shift assignments are indicated.

In Figure 6 are compared the H1′ to H2′/H2″ regions of the 200 ms NOESY spectra of ds11B$_{dia}$ and ds11B$_{para}$. Qualitatively, one can see that the presence of the unpaired electron simplifies the spectral region. Cross-peaks originating for proton pairs proximal to the unpaired electron are no longer observed. For cross-peaks in this and two other spectral regions containing strongly coupled proton pairs (H8/H6 to H2′/H2″/CH_3 and H5 to H6), the change in NOESY intensity due to the unpaired electron was quantitated and converted to an electron−proton distance as described in the Experimental Section. These electron−proton distances are depicted, superimposed on canonical B-form DNA, in Figure 7A; the restraints shown in Figure 7B (upper bound violations of 3−6 Å) cannot be accommodated by this classical structure.

(43) den Hartog, J. H. J.; Altona, C.; van Boom, J. H.; van der Marel, G. A.; Haasnoot, C. A. G.; Reedijk, J. *J. Biomol. Struct. Dyn.* **1985**, *2*, 1137−1155.

(44) den Hartog, J. H. J.; Altona, C.; Chottard, J.-C.; Girault, J.-P.; Lallemand, J.-Y.; de Leeuw, F. A. A. M.; Marcelis, A. T. M.; Reedijk, J. *Nucleic Acids Res.* **1982**, *10*, 4715−4730.

(45) Sherman, S. E.; Gibson, D.; Wang, A. H.-J.; Lippard, S. J. *J. Am. Chem. Soc.* **1988**, *110*, 7368−7381.

(46) Bertini, I.; Luchinat, C. *Coord. Chem. Rev.* **1996**, *150*, 77−110.

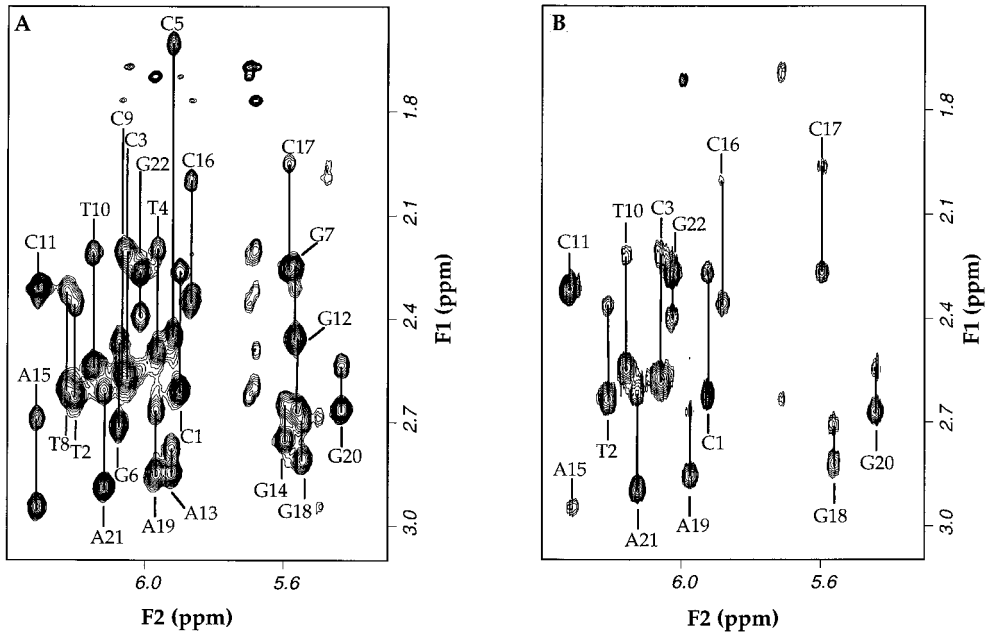

Figure 6. H1′ to H2′/H2″ region of the 200 ms NOESY spectra of (A) 3′ds11$_{dia}$ and (B) 3′ds11$_{para}$. Assignments in the H1′ dimension are indicated.

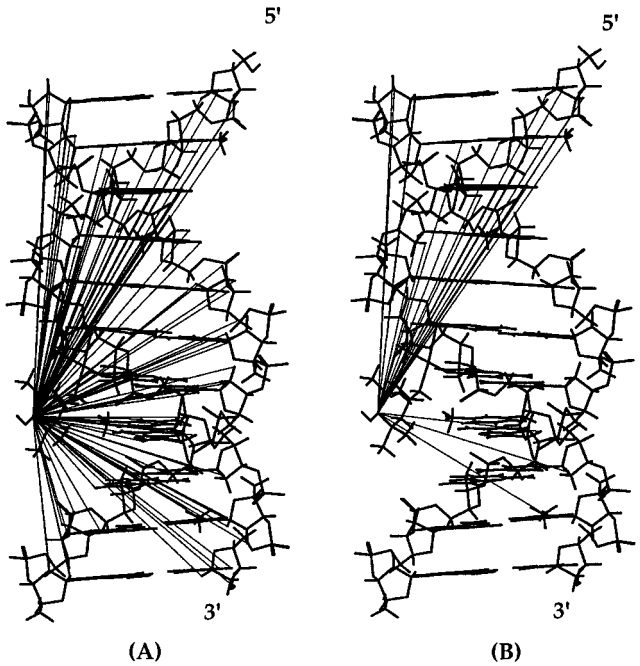

Figure 7. 3′ds11$_{dia}$ represented in a canonical B-type helix form, with superposition of (A) all long-range distance restraints and (B) the subset of long-range distance restraints with upper bound violations. The termini of the platinum-modified strand are indicated.

(E) Structural Implications from the Paramagnetic Data. As just illustrated (Figure 7B), the long-range electron−proton distance restraints are not compatible with a canonical B-form DNA structure. The upper bound violations indicate that the 5′ end of the duplex must be closer to the platinum lesion in the major groove in order to satisfy the restraints. These paramagnetic NMR data for ds11B thus provide direct experimental evidence that the platinum-modified DNA is significantly bent toward the major groove.

Structure Refinement with NMR-Derived Restraints. Structures were generated in two steps. In an initial rMD step[47] (60−80 ps), hydrogen bonding, dihedral angle, and interproton distance restraints were used to refine A- and B-DNA starting structures to convergence. A total of 311 short-range distance restraints were used in initial structure refinements of ds11B$_{dia}$. Of these restraints, 87 were used to define sugar ring conformations (37 H1′ to H2′/H2″; 26 H1′ to H3′/H4′; 6 H3′ to H4′; 18 H3′ to H2′/H2″), 108 restricted the χ angles (38 H8/H6 to H1′; 45 H8/H6 to H2′/H2″; 24 H8/H6 to H3′; 1 H5 to H2′/H2″), 28 addressed base stacking interactions (13 *n*H8/H6 to (*n*+1)N8/H6; 1 *n*H8 to (*n*+1)H5; 2 *n*H2 to (*n*+1)H1; 3 *n*H1 to (*n*+1)-H2; 6 *n*CH3 to (*n*+1)NHb/NHnb; 1 *n*H1 to (*n*+1)H3; 1 *n*NHnb to (*n*+1)H1), 12 related the two independent strands (3 H2 to H1′; 5 H3 to H1; 4 H1 to NHb), 7 oriented the 4AT ligand with respect to the duplex, and 31 represented various intra- and interresidue methyl-to-proton interactions.

In the final step, structures from this initial rMD were subjected to molecular dynamics refinement restrained with the full relaxation matrix so as to correct for inaccuracies in interproton distances determined by the two-spin model. For this relaxation matrix refinement of the DNA structure, ∼1300 cross-peak volumes of the above assigned peaks from the five NOESY spectra of ds11B$_{dia}$ were tabulated, in order of mixing time for use as interproton restraints in the iterative RELAX function of XPLOR.[15] Two sets of structures were generated. One set was restrained with conventional interproton restraints (denoted dia), and the second set with the addition of the long-range electron−proton distance restraints (denoted dia+para). The RMSDs and R-factors of the final refined structures are listed in Table 3.

In Figure 8, final structures from four representative refinements are overlaid with purple and red indicating dia and dia+para restrained structures, respectively. Both sets of final structures deviate significantly from A- and B-DNA starting structures, although a B-DNA duplex fits the NOESY intensities much better than an A-DNA duplex (Table 3). Significant bending toward the major groove is observed in all structures (Figure 8), as is significant widening of the minor groove near the platinum-modification site (Figure S10). The largest differences in the dia and dia+para restrained structures occur at the ends of the duplex. The 5′ end of the duplex, in particular, is bent more toward the major groove in all dia+para structures

(47) Gronenborn, A. M.; Clore, G. M. *Biochemistry* **1989**, *28*, 5978−5984.

Table 3. RMSDs,[a] R-Factors,[b] and Selected Structural Parameters for Refined Duplexes As Compared to Canonical DNA Forms and Other High Resolution Structures

duplex	RMSD[c] (Å)	R-factor	ρ[d] (deg)	Pt to G base plane distance (Å) 5′-G	3′-G
A-DNA		12.7			
B-DNA		7.9			
dia	1.16	6.24[c]	47	0.7	0.6
dia+para	1.12	6.08[c]	50	0.5	0.6
cisplatin-dodecamer crystal structure[e]			28	1.3	0.8
cisplatin-dodecamer NMR structure[f]			49	0.8	0.8
cisplatin-octamer NMR structure[g]			26	1.0	0.8

[a] Root-mean-squared deviation of all non-hydrogen atoms in six final structures. [b] Sixth-root residuals calculated as described by Brünger.[15] [c] Mean of R-factors calculated for six final structures. [d] Average roll (ρ) angle between the two modified guanine bases as calculated by CURVES.[36] [e] Reference 7. [f] Reference 8. [g] Reference 9.

Figure 8. Overlay of dia (purple) and dia+para (red) restrained duplex structures resulting from relaxation matrix refinement. The best fit of the six internal base pairs was used to overlay the structures.

(Figure 8). This difference in the location of the DNA ends is reflected in the RMSD of the dia and dia+para structures, which is 1.5−2.0 Å for the heavy atoms of all 11 base pairs, but only 0.8−0.9 Å when just the central six base pairs are compared.

The large majority of the backbone torsion angles fall within the range observed for A- and B-DNA structures,[48] with only a few α and γ values, predominantly in the central four base pairs, lying outside of these limits (Table S1). Overall, the helical parameters of the dia and dia+para restrained structures are very similar (Table S2). The largest differences in these parameters occur in the T2-A21, C3-G20, and T4-A19 base pairs. Comparisons of selected base pair and base pair step parameters are available in Figure S11. The distortions caused by the bifunctional platinum lesion in these structures include a large positive stretch and buckle at the G6-C17 base pair and significant opening and stagger at the G7-C16 base pair. Both dia and dia+para structures also show significant unwinding (<25° twist), large positive roll (~50°), and increased shift values at the G6-G7 base pair step.

When the H8/H6 to H1′/H5 region of the 200 ms NOESY spectrum (Figure S12) of ds11B$_{dia}$ is compared to those back-calculated from dia and dia+para refined structures, differences between the calculated and observed spectra are subtle. In general, the two sets of predicted spectra agree equally well with the experimental data. Spectral data calculated from both the dia and dia+para structures, however, lack a T10 H6 to C11 H5 cross-peak and, in both, the intensity for the A13 H2 to T10 H1′ cross-peak is too high (Figure S12). In addition, several cross-peak intensities are too weak in the spectrum predicted from the dia structure, including A13 H8 to G12 H1′ and A19 H8 to G18 H1′ (Figure S12).

Discussion

Characterization and Duplex Stability of a Spin-Labeled Platinated Oligonucleotide. The distribution of orientational isomers resulting from modification of ts11 with **1** is the same as that observed[19] for platination of calf thymus DNA with *cis*-[Pt(NH$_3$)(CyNH$_2$)Cl$_2$], the major metabolite of a family of oral Pt(IV) antitumor agents.[20,21,26] Although binding of **1** to the dinucleotide d(GpG) yields equal amounts of both 5′ and 3′ orientational isomers,[18] modification of the single-stranded 11mer under the same conditions results in a significantly greater amount of the 3′ isomer (2:1 ratio of 3′ to 5′). The predominance of this isomer may be attributed to hydrogen bonding between the 5′ amine ligand and the 5′ phosphate of the platinated d(pGpG) unit,[7,45] an interaction that may be sterically hampered by a bulky substituent on the 5′ amine.[19]

Although the 3′ isomer is preferred upon modification of the 11mer sequence with **1**, the melting profiles of the 3′ and 5′ isomeric modified duplexes are the same. Formation of the bifunctional lesion in either orientation decreases the melting temperature by ~24 °C, comparable to values measured for short DNA duplexes modified with cisplatin at a single d(GpG) site.[49] Clearly the distortion caused by the bifunctional adduct provides a more significant energy perturbation to the duplex than any specific interactions with substituents on the modified amine ligand.

Comparisons with Structural Studies of Cisplatin-Modified Oligonucleotides. Several structural elements have previously been identified in DNA modified with cisplatin at the N7 positions of adjacent purine residues.[50] In both single- and double-stranded DNAs, cisplatin modification of adjacent guanosine residues induces a change in the sugar conformation of the 5′ coordinated nucleoside, from $C_{2'}$-endo to $C_{3'}$-endo. There is also disruption of hydrogen bonding and/or increased water

(48) Baleja, J. D.; Pon, R. T.; Sykes, B. D. *Biochemistry* **1990**, *29*, 4828−4839.

(49) Van Hemelryck, B.; Guittet, E.; Chottard, G.; Girault, J.-P.; Huynh-Dinh, T.; Lallemand, J.-Y.; Igolen, J.; Chottard, J.-C. *J. Am. Chem. Soc.* **1984**, *106*, 3037−3039.

(50) Yang, D.; Wang, A. H.-J. *Prog. Biophys. Mol. Biol.* **1996**, *66*, 81−111.

accessibility at the 5′ coordinated G−C base pair, as revealed in several recent NMR solution studies.[8,9,51,52] Detection and assignment of the 5′ dG imino proton has proved to be very difficult, even at reduced temperatures. These structural features are shared by the spin-labeled, platinated undecamer duplex investigated here.

In the crystal structure of d(CCTCTG*G*TCTCC)·(GGA-GACCAGAGG),[7] unconventional hydrogen bonding occurs at the base pair to the 3′ side of the platinum lesion. In particular, the adenine amino group is no longer within hydrogen-bonding distance of its Watson−Crick partner but instead interacts with O6 of guanine in the preceding, platinated base pair. Although there is no direct evidence for such a feature in the NMR solution structure of ds11B_{dia}, the imino proton in the corresponding T−A pair (T8 H3) is very broad, and the unidentified cross-peak to G7 H1 in the preceding base pair could possibly arise from such an unconventional hydrogen-bonding scheme.

Data from early NMR studies[43] indicated that the unmodified decamer duplex, d(TCTCGGTCTC)·(GAGACCGAGA), adopts a right-handed, B-form helical structure in solution. The unmodified 11 bp sequence used in the present study, which has an identical sequence except for an additional C−G base pair at the 5′ end, is similarly expected to have B-form character. Any deviations from B-DNA would have to result from platinum modification. NOESY cross-peak intensities between both exchangeable and nonexchangeable proton pairs in ds11B_{dia} differed by the greatest extent from those expected for B-form DNA near the site of platination. The most significant changes in chemical shifts reported upon platination of the corresponding decamer with cisplatin were similarly restricted to the central four base pairs.[43]

The final structures of 3′ds11, refined with dia and dia+para restraints, show both similarities and differences to the structures of a cisplatin-modified dodecamer in the crystal[7] and the dodecamer and octamer duplexes studied by NMR in solution.[8,9] The minor groove widths of all four duplexes (Figure S10) widen near the platinum lesion, the magnitude of which is comparable for the dia, dia+para, and dodecamer structures (maximum ∼10−11 Å) but significantly less in the octamer duplex (∼7−8 Å). The widened minor groove, particularly near the platinum coordination site, has been implicated in the recognition of platinated DNA duplexes by HMG-domain proteins.[7] Since 10−11 Å minor groove widths are observed in the dia and dia+para structures reported here as well as in the dodecamer crystal and solution structures, this feature can be confidently attributed to formation of the platinum 1,2-intrastrand cross-link rather than arising from crystal packing forces unique to the solid state.

Figure 9 displays the structures of the cisplatin-modified DNAs as determined in the dia+para NMR study and by X-ray crystallography. Since the sequences of the two modified duplexes are not identical, the view chosen in the figure represents the best superposition of non-hydrogen atoms in the platinum coordination sphere, the coordinated guanine bases, and the sugar−phosphate backbone (...-P−O5′−C5′−C4′−C3′−O3′-...). The overall topologies of the two structures are remarkably similar, with an RMSD of 1.98 Å for the atoms described. Comparisons of the dodecamer crystal structure to the dia NMR, dodecamer NMR, or octamer NMR structures result in corresponding RMSDs of 2.26, 3.80, and 2.78 Å, respectively. Details of the similarities and differences between the crystal and solution structures of the dodecamer are discussed elsewhere.[8] Visual inspection of the dodecamer crystal and dia+para NMR structures reveals comparable directions and magnitudes of curvature (Figure 9, top). In the solid state, the duplex dodecamer is predominantly an A-form helix, exhibiting a wide central hole when viewed down its 5′ end.[7] This characteristic feature of A-DNA is also clearly evident when the dia+para NMR structure is viewed in a similar manner (Figure 9, center). The central hole arises even though only two of the 22 sugar residues in this duplex have A-type ($C_{3'}$-endo) sugar puckers. The global helix axis, as determined in the program CURVES,[36,37] passes through the center of this hole at the 5′ end of the dodecamer crystal structure but through the base pairs in the corresponding portion of the dia+para NMR structure. Because the helical axes of these two very similar duplexes are so differently defined in CURVES (Figure S13), the bend angle as determined by the program for the dodecamer is ∼40°, whereas a much larger value results for the undecamer structure (∼80°). As described previously, bend angle analysis is facilitated by the determination and use of local helix axes.[7] As with the global helix axes, these local axes are also defined very differently for the dodecamer X-ray and the dia+para NMR structures, resulting again in large differences in bend angle values calculated for the two duplexes. Despite the difficulty in rigorously calculating and using bend angles to compare these duplex structures, their overall shapes are clearly very similar with substantial bending of the duplex toward the major groove (Figure 9). By comparison, gel mobility assays, which reflect macroscopic duplex shape, afford bend angles of 32−34° for such adducts.[40]

The similarities between the dia+para NMR and dodecamer X-ray duplex topologies do not extend to the roll angle (ρ) between the platinated guanine base ring planes. Although a positive roll is observed in all five structures analyzed (Table 3), the magnitudes are significantly larger for the dia, dia+para, and dodecamer NMR structures. The roll angles observed in the dodecamer crystal and octamer NMR structures are accompanied by greater displacements of the platinum atom from the planes of the 5′ guanine bases (Table 3). These displacements may be related to the identity of the DNA flanking base pairs. In both the dodecamer and octamer structures, the internal sequence is d(TpGpG)·d(CpCpA), whereas the sequence in the present study is d(CpGpG)·d(CpCpG). It is possible that the 5′ CG step, which has been reported to have a large wedge angle,[53] can modulate the roll of the platinated d(GpG) site. Another possible source for the roll angle differences is the nature of the platinum compound. The presence of a bulky substituent on the amine ligand in the major groove may affect the relative orientations of the modified guanine bases, even though the nitroxide group is positioned toward the 3′ side of the lesion.

Effects of Paramagnetic Distance Restraints on Structure Refinement. NMR data for duplex DNA modified with cisplatin at a d(GpG) site have previously been interpreted as evidence for a localized distortion of the duplex, such as a kink, rather than a more gradual change in structure.[9,43,51] These earlier studies employed conventional NMR NOESY data, however, which reflect mainly nearest neighbor interactions (<5 Å) and are limited in their ability to characterize more global changes in duplex structure. Although many small localized alterations in a predominantly linear DNA may result in a significant distortion of the global helix topology, such individual changes may be well within the error of interproton

(51) Herman, F.; Kozelka, J.; Stoven, V.; Guittet, E.; Girault, J.-P.; Huynh-Dinh, T.; Igolen, J.; Lallemand, J.-Y.; Chottard, J.-C. *Eur. J. Biochem.* **1990**, *194*, 119−133.

(52) de los Santos, C.; Patel, D. J. Personal communication.

(53) Hartmann, B.; Lavery, R. *Q. Rev. Biophys.* **1996**, *29*, 309−368.

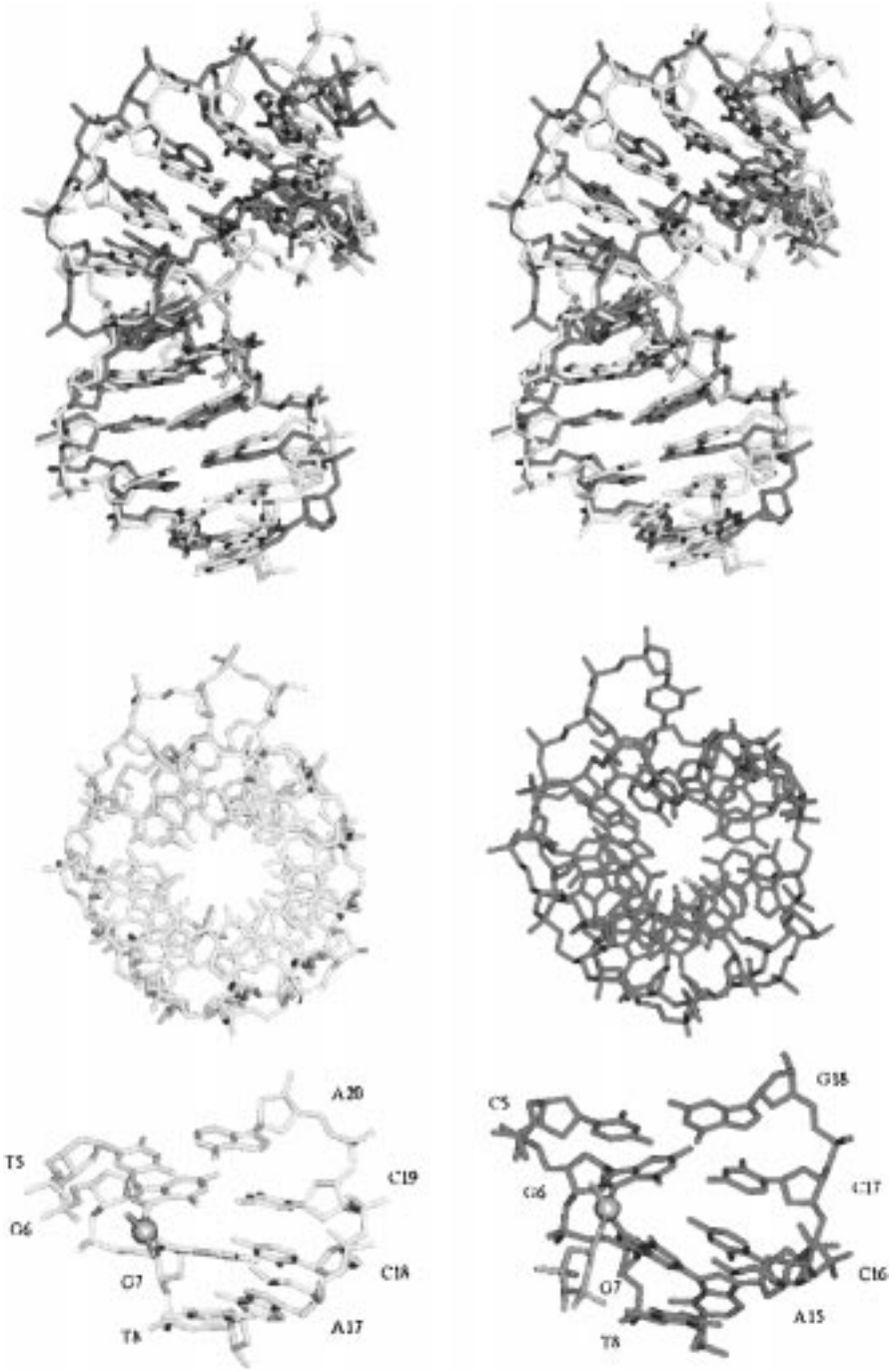

Figure 9. At the top: Stereoviews of the cisplatin-modifed dodecamer crystal structure (yellow) and the dia+para restrained NMR structure (red). In the center: The same duplexes are oriented such that the 5′ axis is directed toward the viewer. At the bottom: The central 4 bp of each duplex are shown from the major groove. In all views of both duplexes, the platinum coordination sphere is gray.

distance or dihedral angle determinations. The long-range electron−proton distance restraints described in the present paramagnetic NMR investigation address this deficiency and allow for a clearer picture of the platinum-induced alterations throughout a full turn of the DNA double helix.

The application of nitroxide spin labels to biological macromolecular structure determination has a rich history,[38,54] but most of this work has focused on proteins and protein−ligand interactions. The early need for the additional structure restraints afforded by nitroxide spin labels, however, was later superseded by technical advances in multidimensional and multinuclear NMR methods. These advances have allowed for the determination of high-resolution protein structures in solution in the absence of long-range paramagnetic restraints,[17] since protein folding brings nonadjacent residues inside the 5 Å NOESY window. The persistent lack of nonnearest neighbor restraints in duplex oligonucleotides, which do not form folded globular protein-like structures, has made it difficult to obtain well-determined structures in a similar manner. To our knowledge, this is the first study in which data from a covalently attached nitroxide spin label has been used to refine the global structure of any duplex oligonucleotide in solution.

Introduction of the 4AT ligand to afford long-range distance restraints, first applied to refine the solution structure of a

(54) *Spin Labeling II*: *Theory and Applications*; Berliner, L. J., Ed.; Academic Press: New York, 1979; pp 291−345.

platinum-modified single-stranded dinucleotide monophosphate,[18] has contributed to our understanding of the present platinum-modified duplex undecamer in several ways. Visual inspection of the long-range distances restraints mapped onto a canonical B-form undecamer duplex clearly illustrate that the DNA, particularly at the 5′ end of the duplex, must bend substantially toward to major groove in order to accommodate the data (Figure 7B). Such a conclusion would have been difficult, if not impossible, to make from visual inspection of a series of short-range interproton distances. The addition of the paramagnetic restraints in duplex structure refinement did not affect the agreement of the final structure with the conventional diamagnetic data. Instead, both dia and dia+para restrained refinements of this duplex yielded structures that comparably converged from A-form and B-form starting structures and that agreed equally well with the NOESY intensity buildup data (Table 3). In addition, only subtle differences were observed in NOESY data back-calculated from either the dia or dia+para structures (Figure S12). This evidence together with the very similar helical parameters of the duplexes resulting from these two sets of refinements (Figure S11) indicates that the same local structure is achieved from both the dia and dia+para restraints.

Finally, although all long-range distance restraints are satisfied in the dia+para refined structures, approximately 25−30 long-range distance restraints are violated in each dia structure, the upper-bound sum of which is greater than 45−50 Å. Agreement with all long-range distance restraints, a result of dia+para refinement, produces duplex structures with an overall shape comparable to that of the cisplatin-modified dodecamer structure determined by X-ray methods. The changes in refined undecamer duplex structure resulting from the inclusion of the long-range distance restraints may reflect gradual changes in duplex morphology that are poorly addressed by conventional NMR observables.

Conclusion

The addition of a large number (∼100) of conservative long-range electron−proton distance restraints has resulted in a solution structure of a nitroxide spin-labeled, platinum-modified DNA duplex that agrees with interproton restraints in the diamagnetic analogue but could not be deduced from the latter restraints alone. Although the nitroxide spin label was introduced in the form of a platinum ligand for this study, others have developed methods whereby such a label is attached directly to a DNA residue through either a covalent base[42,55] or a phosphate modification.[56] By employing such methods, long-range distance restraints might be similarly determined for other noncanonical DNA structures, for example, A-tracts (dA_n where $n \geq 3$), the overall shapes of which (including magnitude and direction of bending) have been difficult to characterize by conventional diamagnetic NMR methods.[16,53,57] The use of spin labels in DNA, particularly for duplexes modified with cisplatin and related drugs, may also significantly facilitate the characterization of ternary complexes formed with other macromolecules. With the aid of such NMR-derived long-range distance determinations, it might be possible to identify structural features required for the recognition of platinated DNA in the cell, with the ultimate aim of establishing a link between DNA structure modification and the cytotoxic mechanism of platinum antitumor agents.

Acknowledgment. This work was supported by Grant CA34992 from the National Cancer Institute. NMR instrumentation was made available at the Francis Bitter Magnet Laboratory at MIT, which is supported in part under NIH Grant RR0095. S.U.D. is grateful to the NIH for a postdoctoral fellowship. We thank C. Luchinat and I. Bertini (University of Florence) for valuable discussions, assistance with preliminary T_2 relaxation data collection on paramagnetic samples, and financial support of S.U.D. and S.U.D. to obtain these data.

Supporting Information Available: Tables S1 and S2 reporting backbone parameters for diamagnetic and diamagetic and paramagnetic refinements; Figures S1−S13 showing electron−proton distance dependence of paramagnetic relaxation rates; HPLC trace of separated products of reaction of ts11 with **1**; EPR spectrum of $ds11B_{para}$; HPLC trace of enzymatically digested reaction products; UV−vis melting and cooling curves; NOESY spectra; minor groove width measurements; plots of helical base pair parameters; and calculation of global helical axes, (21 pages, print/PDF). See any current masthead page for ordering information and Web access instructions.

JA9742592

(55) Kryak, D. D.; Bobst, A. M. *Nucleosides Nucleotides* **1990**, *9*, 1015−1019.

(56) Nagahara, S.; Murakami, A.; Makino, K. *Nucleosides Nucleotides* **1992**, *11*, 889−901.

(57) Harvey, S. C.; Dlakic, M.; Griffith, J.; Harrington, R.; Park, K.; Sprous, D.; Zacharias, W. *J. Biomol. Struct. Dyn.* **1995**, *13*, 301−307.